PHYSICAL REVIEW D VOLUME 47, NUMBER 5 1 MARCH 1993

Direct-photon production in heavy-ion collisions

A. Petridis
Department of Physics and Astronomy and Ames Laboratory–Department of Energy, Iowa State University, Ames, Iowa 50011

K. E. Lassila
Department of Physics and Astronomy and Ames Laboratory–Department of Energy, Iowa State University, Ames, Iowa 50011 and Soltan Institute for Nuclear Studies, 00-681 Warsaw, Poland

J. P. Vary
Department of Physics and Astronomy and Ames Laboratory–Department of Energy, Iowa State University, Ames, Iowa 50011
(Received 16 October 1992)

To study plasma photons in relativistic heavy-ion collisions one must account for direct photons from all possible sources. The aim of this work is the examination of the effect that initial-state parton distributions in nuclei, distorted to accommodate the European Muon Collaboration (EMC) effect, will have on the direct-photon spectrum produced relative to the basic QCD subprocesses in free nucleon-nucleon collisions. Since this parton distortion has been quite satisfactorily described by an expansion of the nuclear state in multiquark color-singlet (cluster) basis states, this "quark cluster model" should give useful predictions for the reflection of the EMC effect in the nucleus-nucleus direct photons. The presence of such clusters enhances the phase space available to direct photons. As a result, the direct-photon yield per nucleon shows significant dependence on the photon transverse momentum p_T. The ratio of the cross section per nucleon for zero photon longitudinal rapidity in collisions of two similar heavy nuclei to the cross section for collisions of two free protons exhibits deviations from unity, being less than one for small values of p_T, and larger than one for large values of p_T. We investigate the sensitivity of this ratio on the mass number of the colliding projectiles, on the effective multiquark cluster probability, and on the nucleon or multiquark cluster gluon distributions for various values of the heavy-ion momentum per nucleon.

PACS number(s): 12.38.Mh, 12.38.Qk, 13.85.Qk, 25.75.+r

I. INTRODUCTION

Parton effects in high-energy nuclear physics have attracted the attention of many particle and nuclear physicists in the past few years. Experiments that involve nuclear targets have demonstrated significant differences between the behavior of partons in free hadrons and those bound in nuclei, a result known as the European Muon Collaboration (EMC) effect [1]. Many contributions to the EMC effect have been examined to explain this phenomenon, including nucleon Fermi motion, pions in nuclear matter, the redefinition of the momentum fraction (x) of the parton due to nuclear binding, overlapping of nucleons to form multiquark clusters, overlapping of partons in adjacent nucleons, and others [2–4]. All these potential contributions to the EMC effect need to be examined carefully in as many processes as possible to assess their combined effects with due attention to the possibility of double counting them.

Expanding the nuclear state in multiquark cluster basis states has proved to be extremely reliable in describing a large number of processes beginning with deep inelastic scattering (DIS) on ^{3}He [5]. Among the subsequent applications are those to the DIS EMC effect with large nuclear targets [6,7] and the description of the ^{3}He charge form factor [8]. The distinction between shadowing and antishadowing contributions from clusters at small x was clearly elucidated [7], and shadowing behavior in DIS on a nuclear target of mass number A was shown to imply shadowing in Drell-Yan (DY) lepton pairs produced on A [9]. This follows since both processes have similar sensitivity to the initial-state parton distributions which reflect the EMC effect. The DY processes treated include pairs produced by pion [3] beams and proton [4, 10, 11] beams. Direct-photon production with proton probes on nuclei has also been studied [12].

The underlying physics of the multiquark cluster expansion is most simply illuminated with DIS on the deuteron (^{2}H) [13, 14]. The complete state vector $|^2\mathrm{H}\rangle = \alpha|3q\rangle + \beta|6q\rangle$ gives the probability of finding the neutron (n) and the proton (p) isolated as $|3q\rangle$ clusters or overlapping in a color-singlet six-quark configuration $|6q\rangle$. From the $|6q\rangle$ part of ^{2}H, baryons can emerge backward opposite to the probe direction with large cross sections [15]. The probability that a parton chosen at random from ^{2}H emanates from the $6q$ cluster is $|\beta|^2$.

For A nucleons the general expansion of the nuclear state into orthonormal color-singlet basis states $|n3q\rangle$ would be difficult to carry out:

$$|A\rangle = \alpha|3q\rangle + \beta|6q\rangle + \gamma|9q\rangle + \cdots . \quad (1)$$

For three- and four-nucleon systems, $|\alpha|^2$, $|\beta|^2$, $|\gamma|^2$, etc.,

have been related to microscopic nuclear wave functions, and a simple parametrization was given for extrapolation to heavier systems [16]. This parametrization shows that the probabilities for the higher clusters decrease rapidly, and so we will keep the first two contributions as representative in the following calculations. However, the values in Ref. [16] based on the assumption of a critical radius for cluster formation may be underestimated as nearby nucleons can exchange quarks [17]; such an extended system will be a color singlet and can be part of the $|6q\rangle$ contribution. Further, dynamical support for $6q$ cluster formation in nuclei has also been obtained in Ref. [18]. Altogether, then, it seems a reasonable approximation to a full multiquark cluster expansion of a nuclear state to take the leading $|3q\rangle$ and $|6q\rangle$ configurations as the main source of nuclear partons. Viewed phenomenologically, the $|6q\rangle$ term assimilates many essential features of other contributions, including parton exchange [17] and recombination [19] processes between $|3q\rangle$ clusters which contribute to reactions with external probes.

In principle, direct-photon production in fixed target experiments should give useful information on gluon distributions [20, 21]. However, nuclear effects must be taken into account as the gluon distribution in the nucleus will be shadowed at small x and grow at large x relative to the distribution in the proton [12, 14]. This same nuclear distortion should then exist in direct-photon production in nucleus-nucleus collisions.

In this work we expand our investigation on direct-photon production to collisions that involve two high-energy heavy nuclei. To guide future experiments at the BNL Relativistic Heavy Ion Collider (RHIC) and elsewhere, it is important to know the photon production rate coming directly from the hard QCD process, including modifications due to nuclear effects, in order to isolate the thermal photons [22] which are predicted to emerge during the formation of a quark-gluon plasma. In addition, better insight regarding the poorly determined gluon distributions may be developed since the latter play a dominant role in the production of direct photons.

This article is organized as follows. Sections II–IV lay out the essentials of the quark cluster model (QCM). The parton distributions in quark clusters are defined and related to one another by isospin invariance considerations, and the effective probability for six-quark cluster formation in a nucleus is discussed. Section V introduces the kinematics of nucleus-nucleus collisions and the cross sections for direct-photon production at the partonic and the nuclear level with reference to the nonperturbative hadronic flux factors involved. The form of these functions is given in the Appendix. Section VI presents our numerical results for the direct-photon production cross section at zero photon longitudinal rapidity for various nuclei, energies, and quark cluster probabilities as a function of the photon transverse momentum (p_T). Section VII extracts the nuclear dependence by evaluating ratios of cross sections and examines the sensitivity of the expected nuclear effects to the parameters of our model. Section VIII gives an interpretation of our results and discusses the physical observables.

II. PARTON MOMENTUM DISTRIBUTIONS

A quark cluster is characterized by the number of its valence quarks, N. Clusters are formed by the merging of nucleons, so that $N = 3$ for a single nucleon, $N = 6$ for a six-quark cluster, etc. Operationally, the merger might be defined to occur when the two nucleons approach each other within a critical distance $d_c \approx 1$ fm. We shall first consider six-quark clusters formed from protons and apply isospin (I) relations to obtain the parton distributions for clusters that involve neutrons as well.

The variable x is defined as the fraction of the cluster ($|3q\rangle$ or $|6q\rangle$) momentum carried by a particular parton (valence quark, sea quark, or gluon) in a frame of reference in which the cluster momentum is very large compared to the intrinsic transverse momentum (k_T) of the partons so that the latter can be neglected. This is true in the laboratory frame of reference in relativistic heavy-ion collisions, and so x is a relativistically invariant quantity and ranges from 0 to 1. The probability that a certain parton carries momentum fraction x of its parent cluster, i.e., the *number density* of the parton it represents, is a function of x. It may also depend on the *factorization scale* Q^2 at which the parton distributions are separated from the perturbative QCD part of the interaction, but this Q^2 dependence will tend to cancel in the ratios we shall calculate for heavy-ion collider experiments. The distributions we are going to use have been applied to DIS data with leptons and hadrons on protons and nuclei and successfully describe EMC-type data [4, 7, 9].

A protonlike cluster of type N contains $2N/3$ *up* valence quarks whose momentum distribution is denoted by $U_N(x)$ and $N/3$ *down* valence quarks whose momentum distribution is $D_N(x)$. The *ocean* of the cluster consists of three species of *sea* quarks accompanied by an equal number of antiquarks to maintain electric charge neutrality. Here, we assume that *up* and *down* quarks and antiquarks in the *ocean* have identical distributions $S_N(x)$ and the *strange* sea distribution is $S_N(x)/2$. The total sea or *ocean* distribution is then $O_N(x) = 5S_N(x)$. The gluon distribution is denoted by $G_N(x)$.

We assume simple forms for the momentum distributions:

$$U_N(x) = B_N^u \sqrt{x}(1-x)^{b_N^u}, \tag{2}$$

$$D_N(x) = B_N^d \sqrt{x}(1-x)^{b_N^d}, \tag{3}$$

$$S_N(x) = A_N(1-x)^{a_N}, \tag{4}$$

$$G_N(x) = C_N(1-x)^{c_N}. \tag{5}$$

The number densities will be denoted by lowercase letters. Results of DIS with electron probes on nucleons and with neutrino and antineutrino beams on protons suggest that the exponent of the *down* valence quark distribution in the proton is bigger than that of the *up* valence quark. A simple assumption in concert with this observation is

$$b_N^d = b_N^u + 1. \tag{6}$$

The coefficients and exponents in these expressions are determined by reasonable constraints which are given in

order of decreasing confidence.

(1) *Normalization of valence quark distributions.* The valence number densities should give the appropriate number of valence quarks upon integration over x:

$$\int_0^1 \frac{dx}{x} U_N(x) = \frac{2}{3}N, \quad \int_0^1 \frac{dx}{x} D_N(x) = \frac{1}{3}N. \tag{7}$$

(2) *Momentum sum rule.* The *total* momentum fraction carried by a parton species is

$$x_N^F = \int_0^1 dx\, F(x), \tag{8}$$

where F stands for *up (u), down (d), ocean (o),* or *gluon (g)* momentum distributions. The sum of all the total momentum fractions must be equal to unity:

$$\sum_F x_N^F = 1. \tag{9}$$

(3) *Dimensional counting rules.* The leading behavior of the *up* valence quark momentum distribution in the limit $x \to 1$ suggests that $b_3^u = 3$. Generalizing this idea to any proton type cluster, we may write [5, 7]

$$b_N^u = 2N - 3. \tag{10}$$

(4) *Ocean to gluon momentum ratio.* We assume that the ratio of the total momentum fractions carried by ocean quarks and gluons is independent of N. Based on examination of pion and nucleon data, we shall take [7]

$$x_N^o / x_N^g = 1/5. \tag{11}$$

These assumptions are sufficient to determine the total momentum fractions carried by the various parton species.

(5) *Sea and gluon distribution powers.* In order to determine the complete set of parameters in our model, we need some further information on the *sea* and *gluon* distributions, which, however, are poorly determined by current experiments. Various data suggest that $a_3 = 9$. We shall take $a_6 = 11$. For the *gluon* exponents we shall assume [7]

$$b_N^{u,d} \le c_N \le a_N. \tag{12}$$

We shall take $c_3 = 6$ and $c_6 = 10$ as possible values and investigate the influence of varying these parameters by ± 1.

Powers of $(1 - x)$ for the three- and six-quark cluster distribution functions are listed in Table I. The sea and gluon distributions are proportional to the total momentum fractions carried by them. Any change in the exponents of the sea or gluon distributions affects only their shape but not the corresponding total momentum fraction. As N increases the total momentum fraction carried by valence quarks decreases while the total momentum fraction carried by the ocean quarks and by the gluons increases. The momentum fractions calculated with the power values given in Table I are listed in Table II. We note that the fraction of momentum carried by the gluons in a proton is somewhat higher than some recent [23] determinations. In the ratios we shall present, however, effects due to this difference will tend to be very minor.

TABLE I. Powers of $(1 - x)$.

	$N = 3$	$N = 6$
a_N	9	11
c_N	6	10
b_N^u	3	9
b_N^d	4	10

TABLE II. Total momentum fractions carried by partons in three- and six-quark clusters. The superscripts u, d, v, s, o, and g refer to up, down, valence, sea, ocean, and gluon, respectively.

	$N = 3$	$N = 6$
x_N^u	0.222	0.190
x_N^d	0.091	0.087
x_N^v	0.313	0.277
x_N^s	0.023	0.024
x_N^o	0.114	0.120
x_N^g	0.572	0.602

III. ISOSPIN INVARIANCE RELATIONS

From protonlike clusters, clusters with neutrons will be obtained from obvious isospin relations. For u and d quark distributions in a proton (p) or neutron (n),

$$U_p(x) = D_n(x) \equiv U_3(x), \quad D_p(x) = U_n(x) \equiv D_3(x). \tag{13}$$

A cluster of two protons (pp) or two neutrons (nn) belongs to the $I = 1$ state, and the analogous relations to Eq. (13) are

$$U_{pp}(x) = D_{nn}(x) \equiv U_6(x), \quad D_{pp}(x) = U_{nn}(x) \equiv D_6(x). \tag{14}$$

A proton and a neutron (pn) cluster may be in a mixture of $I = 1$ or $I = 0$, with the triplet component related to the (pp)-type cluster. A reasonable assumption for the $I = 1$ (pn) cluster is

$$U_{pn}^{(1)}(x) = D_{pn}^{(1)}(x) = [U_{pp}(x) + D_{pp}(x)]/2, \tag{15}$$

where the superscript (1 or 0) refers to the isospin value. The $I = 1$ state distributions are assumed the same as the $I = 0$ ones for simplicity:

$$\begin{aligned} U_{pn}(x) = D_{pn}(x) &= U_{pn}^{(1,0)}(x) = D_{pn}^{(1,0)}(x) \\ &= [U_6(x) + D_6(x)]/2. \end{aligned} \tag{16}$$

For fixed N, the sea and the gluon distributions are taken independent of isospin. This section can also be applied to clusters with more than six valence quarks.

IV. MULTIQUARK CLUSTER PROBABILITIES

An important ingredient to this model is the probability of the formation of multiquark clusters in the nuclear medium. In previous work, this probability has been calculated for clusters of various numbers of valence quarks based on realistic or semirealistic nuclear wave functions [5, 16]. Another approach is to consider such probabilities as free parameters to be fixed by comparison with data from scattering experiments involving nuclei. In the case of the deuteron, which can form only a (pn)-type six-quark cluster, both approaches seem to agree on a value approximately between 0.04 and 0.05 [14]. This is also in agreement with data on the production of backward hadrons from deuterium targets [15]. In more massive nuclei larger clusters may also be formed. We define the *effective* probability f for the formation of six-quark clusters to incorporate the presence of heavier clusters. A natural question is whether this effective probability has any approximate, simple dependence on the mass number of the nucleus (A). If we use the fact that the nuclear central mass density is approximately constant in A (with the exception of some light but very dense nuclei) and that the volume of the nucleus is proportional to A, we deduce that the effective probability for two nucleons to overlap sufficiently to form a six-quark cluster is $f = c \ln A$ with $c = 0.0575$–0.0721, where we used 0.04 and 0.05 for the deuteron as starting values [12]. This is consistent with the weak dependence of cluster probabilities on A given in Ref. [16]. We shall further test the sensitivity of our results to the value of f.

It is desirable to have an estimate of the average number of the various cluster types in the nucleus because these numbers enter in cross section evaluations. For a nucleus with mass number A, atomic number Z, and "neutron" number $N = A - Z$, the average numbers of (p), (n), (pp), (pn), and (nn) type clusters are denoted by n_p, n_n, n_{pp}, n_{pn}, and n_{nn}, respectively. The following conditions apply to these numbers [3, 24].

(1) *Baryon number conservation.* The sum of all the cluster baryon numbers should be equal to A:

$$n_p + n_n + 2n_{pp} + 2n_{pn} + 2n_{nn} = A. \tag{17}$$

(2) *Electric charge conservation.* The electric charge carried by the clusters must add up to the total charge of the nucleus:

$$n_p + n_{pn} + 2n_{pp} = Z. \tag{18}$$

(3) *Probability conservation.* The total number of clusters of a particular size must be proportional to the corresponding probability:

$$(1-f)(n_{pp} + n_{pn} + n_{nn}) - f(n_p + n_n) = 0. \tag{19}$$

(4) *Clusters in large nuclei.* We assume that, for large nuclei, in which we are mostly interested, the number of each cluster type is proportional to the corresponding nucleon number raised to a power equal to the number of protons or neutrons it contains:

$$\frac{n_p}{Z} = \frac{n_n}{N}, \quad \frac{n_{pp}}{Z^2} = \frac{n_{pn}}{2ZN} = \frac{n_{nn}}{N^2}. \tag{20}$$

The factor of 2 in front of ZN reflects the fact that in an isoscalar nucleus the probability for forming a (pn) cluster is twice as large as the probability for forming a (pp) or an (nn) cluster. We assume this also for nonisoscalar nuclei.

A solution that satisfies all these conditions is

$$n_p = \left(\frac{1-f}{1+f}\right) Z, \quad n_n = \left(\frac{1-f}{1+f}\right) N, \tag{21}$$

$$n_{pp} = \left(\frac{f}{1+f}\right) \frac{Z^2}{A}, \quad n_{pn} = \left(\frac{f}{1+f}\right) \frac{2ZN}{A}, \quad n_{nn} = \left(\frac{f}{1+f}\right) \frac{N^2}{A}. \tag{22}$$

Finally, the total three- and six-quark cluster numbers are

$$n_3 = n_p + n_n = \left(\frac{1-f}{1+f}\right) A, \quad n_6 = n_{pp} + n_{pn} + n_{nn} = \left(\frac{f}{1+f}\right) A. \tag{23}$$

In the case of the deuteron we take $n_6 = n_{pn}$.

V. KINEMATICS AND CROSS SECTIONS

In this section we discuss the direct-photon production process. In our model there are four possible types of hadronic interactions in nucleus-nucleus collisions. We use the index (i) to denote a hadron in the nucleus that moves in the positive z direction and the index (j) to denote a hadron in the nucleus moving in the opposite direction. Those indices take on the value $i, j = 3$ if the hadron is a $|3q\rangle$ state and the value $i, j = 6$ if it is a $|6q\rangle$ state. We categorize those interactions as follows: (a) nucleon-nucleon interactions ($i = 3, j = 3$), whose contribution to the cross section is proportional to $(1-f)^2$; (b) nucleon-$6q$ cluster interactions ($i = 3, j = 6$), with contribution going as $(1-f)f$; (c) $6q$ cluster-nucleon interactions ($i = 6, j = 3$), contributing as $f(1-f)$; (d) $6q$ cluster-$6q$ cluster interactions ($i = 6, j = 6$), proportional to f^2. Cases (b) and (c) are similar but must be treated separately due to their dependence on the kinematic variables. In Fig. 1 we show the general diagram for case (d). Since the mass of a $6q$ cluster is approximately twice the mass of a nucleon and all $3q$ and $6q$ clusters in the nucleus move at the same velocity, the longitudinal momentum of a single nucleon is $\pm P_{\rm lab}$ and that of a $6q$ cluster is $\pm 2P_{\rm lab}$. For the present investigation we neglect the Fermi motion of clusters in the nucleus relative to their motion in the laboratory. In addition, we argue that in a given cluster's rest frame the Lorentz-contracted collision partners interact with it in a time frame that is short compared to the natural response time of the cluster. Hence, we assume the multiple collision process on a given cluster is a set of independent successive impulses on the same initial state configuration—akin to a conven-

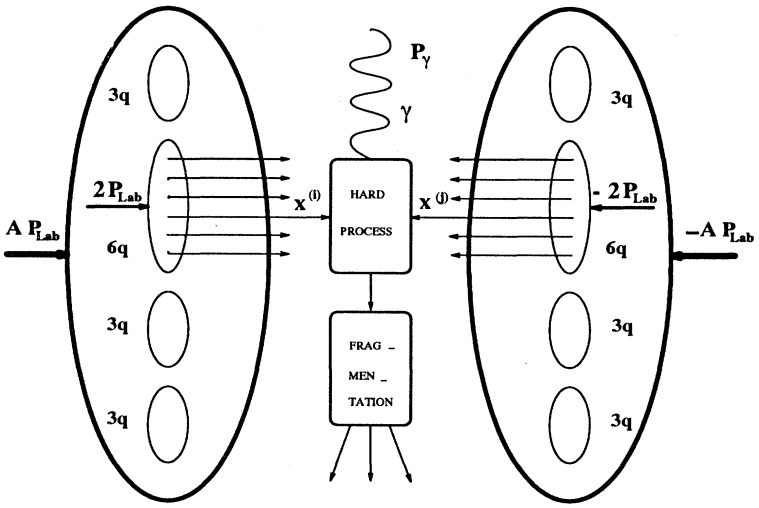

FIG. 1. Six-quark cluster interaction in nucleus-nucleus collision leading to direct photon production.

tional "frozen nucleus" approximation. We also assume incoherence in all cluster-cluster collision processes.

Our goal is to estimate the yield of "primary" (direct) photons, i.e., those emanating from the initial-state multiple collision process, and to leave out completely those photons resulting from subsequent scatterings or decay of secondary fragments. Understanding all photons is of great interest as some may carry important information on the possible formation of quark-gluon plasma [22]. It is our hope that, elucidating the primary photon yield, we will clarify the secondary photon signals. We argue that, at the very least, one should obtain a *quantitative* understanding of the hard photon yield where the processes we treat should dominate before developing strong conclusions from the softer photons where a multitude of processes are expected.

The kinematic invariants that pertain to the four types of hadron interactions mentioned above are

$$s^{(i,j)} = \left(P^{(i)} + P^{(j)}\right)^2 \simeq 2P^{(i)} \cdot P^{(j)}, \tag{24}$$

$$t^{(i)} = \left(P^{(i)} - P_\gamma\right)^2 \simeq -2P^{(i)} \cdot P_\gamma, \tag{25}$$

and

$$u^{(j)} = \left(P^{(j)} - P_\gamma\right)^2 \simeq -2P^{(j)} \cdot P_\gamma, \tag{26}$$

where $P^{(i)}$ and $P^{(j)}$ are the four-momenta of the hadrons,

$$P_\gamma = (E_\gamma, \mathbf{p}_\gamma) = (E_\gamma, \mathbf{p}_T, p_z), \; E_\gamma = \sqrt{p_T^2 + p_z^2} \tag{27}$$

is the four-momentum of the real photon, and the squares of the cluster masses have been ignored.

The longitudinal momentum fraction of a parton relative to its parent hadron moving in the positive z direction is $x^{(i)}$, and $x^{(j)}$ is that for a parton moving in the negative z direction. These fractions are equal to unity when the parton carries the entire momentum of its parent hadron.

In the following all the symbols with carets refer to parton level quantities. The four-momenta of the partons that participate in the hard process ignoring transverse momenta are then

$$\hat{P}^{(k)} = x^{(k)} P^{(k)}, \tag{28}$$

where (k) stands for either (i) or (j). The partons are considered massless. The parton level kinematic invariants are

$$\hat{s}^{(i,j)} = \left(\hat{P}^{(i)} + \hat{P}^{(j)}\right)^2 \simeq 2\hat{P}^{(i)} \cdot \hat{P}^{(j)} = x^{(i)} x^{(j)} s^{(i,j)}, \tag{29}$$

$$\hat{t}^{(i)} = \left(\hat{P}^{(i)} - P_\gamma\right)^2 \simeq -2\hat{P}^{(i)} \cdot P_\gamma = x^{(i)} t^{(i)}, \tag{30}$$

and

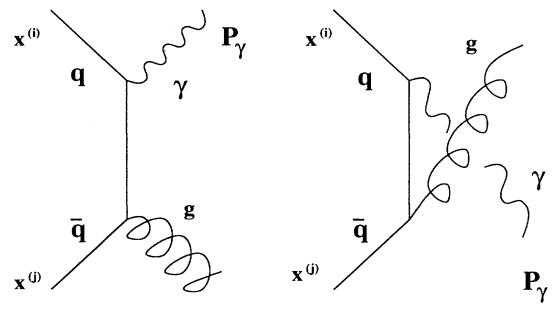

FIG. 2. Direct-photon production diagrams for pair annihilation of a quark and an antiquark.

$$\hat{u}^{(j)} = \left(\hat{P}^{(j)} - P_\gamma\right)^2 \simeq -2\hat{P}^{(j)} \cdot P_\gamma = x^{(j)} u^{(j)}. \quad (31)$$

The dominant hard processes that contribute to direct-photon production are (1) quark-antiquark annihilation ($q\bar{q}$) and (2) quark-gluon Compton-type scattering (qg), shown in Figs. 2 and 3. To lowest order in QCD the corresponding differential cross sections, including color factors, are [25]

$$E_\gamma \frac{d\hat{\sigma}_{q\bar{q}}^{(i,j)}}{d^3p_\gamma} = +\frac{8}{9}\alpha\alpha_s(Q^2)\frac{1}{\hat{s}^{(i,j)}}\left[\frac{\hat{t}^{(i)}}{\hat{u}^{(j)}} + \frac{\hat{u}^{(j)}}{\hat{t}^{(i)}}\right]\delta\left(\hat{s}^{(i,j)} + \hat{t}^{(i)} + \hat{u}^{(j)}\right), \quad (32)$$

$$E_\gamma \frac{d\hat{\sigma}_{qg}^{(i,j)}}{d^3p_\gamma} = -\frac{1}{3}\alpha\alpha_s(Q^2)\frac{1}{\hat{s}^{(i,j)}}\left[\frac{\hat{u}^{(j)}}{\hat{s}^{(i,j)}} + \frac{\hat{s}^{(i,j)}}{\hat{u}^{(j)}}\right]\delta\left(\hat{s}^{(i,j)} + \hat{t}^{(i)} + \hat{u}^{(j)}\right), \quad (33)$$

where $\alpha = 1/137$ is the electromagnetic coupling constant (the squares of the quark charges are not included in these expressions). The running strong coupling constant is

$$\alpha_s(Q^2) = \frac{12\pi}{(33 - 2n_f)\ln\left(\frac{Q^2}{\Lambda^2}\right)}, \quad (34)$$

where $n_f = 3$ is the number of active quark flavors and $\Lambda = 100$ MeV is the QCD renormalization scale constant. To avoid large logarithmic terms due to higher order corrections in the hard part of the interaction, we pick $Q^2 = p_T^2$ [tests of the sensitivity to this choice suggest ($\frac{1}{4}$ to 4)p_T^2 [26]].

In order to calculate the hadron level cross section, we must convolute the parton level cross sections with the appropriate probability flux factors for the partons entering the hard process. These factors express the combined probability that the momentum fractions carried by the interacting partons are equal to $x^{(i)}$ and $x^{(j)}$. We also include the squares of the quark charges in these functions. There are four terms in the hadron level cross section, each corresponding to one of the four cases of hadron interactions and each includes two flux factors for each hard process which we refer to as hadronic structure functions. We assume that there is negligible dependence of these functions on Q^2 in the kinematic domain we are going to consider, so that they explicitly depend only on $x^{(i)}$ and $x^{(j)}$. Moreover, and in the ratios we will present, the Q^2 dependence would largely tend to cancel.

We adopt the notation $H_{q\bar{q}}^{(i,j)}$ for the quark-antiquark annihilation functions and $H_{qg}^{(i,j)}$ for those that correspond to quark-gluon scattering. With these considerations the hadron level cross section is

$$E_\gamma \frac{d\sigma}{d^3p_\gamma} = \sum_{i,j=3,6}\int dx^{(i)}\int dx^{(j)}\left[H_{q\bar{q}}^{(i,j)}(x^{(i)},x^{(j)})\,E_\gamma\frac{d\hat{\sigma}_{q\bar{q}}^{(i,j)}}{d^3p_\gamma} + H_{qg}^{(i,j)}(x^{(i)},x^{(j)})\,E_\gamma\frac{d\hat{\sigma}_{qg}^{(i,j)}}{d^3p_\gamma}\right]. \quad (35)$$

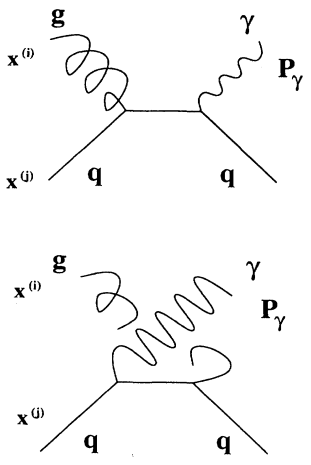

FIG. 3. Direct-photon production from quark-gluon Compton scattering diagrams.

The upper integration limits are equal to unity. One set of integrations can be performed trivially with the δ functions in Eq. (33). We choose to do the integration over $x^{(j)}$. This results in a multiplicative factor $1/(x^{(j)}s^{(i,j)} + t^{(i)})$ and a constraint that relates $x^{(i)}$ to $x^{(j)}$:

$$x^{(i)} = \frac{-x^{(j)}u^{(j)}}{x^{(j)}s^{(i,j)} + t^{(i)}}. \quad (36)$$

The lower limit of the integration over $x^{(i)}$ becomes

$$x_{\min}^{(i)} = \frac{-t^{(i)}}{u^{(j)} + s^{(i,j)}}, \quad (37)$$

which corresponds to $x^{(j)} = 1$. The remaining integrations can be done numerically. All the nonperturbative information is contained in the hadronic structure functions which, also, include the effects of multiquark cluster formation. Their explicit forms are given in the Appendix.

VI. CROSS SECTIONS FOR $y = 0$

In this section we apply our model to numerically calculate the direct-photon production cross section in nucleus-nucleus collisions for zero photon longitudinal rapidity ($y = 0$). In this case the photon is emitted perpendicular to the beam direction ($p_z = 0$) with transverse momentum p_T. High values of p_T can be reached due to the on-mass-shell condition for the real photon ($m^2 = 0$). A useful relativistically invariant variable is the ratio of twice the transverse momentum of the photon to its maximum value in the nucleon-nucleon collision case:

$$x_T = \frac{2p_T}{\sqrt{s^{(3,3)}}} = \frac{p_T}{P_{\rm lab}}. \tag{38}$$

The last equality is valid when $y = 0$. We shall use gold ($A = 197$, $Z = 79$) as a sample nucleus to illustrate our results. Based on the cumulative experience in previous applications, the six-quark cluster probability for gold (Au) is expected in the range 0.30–0.38. We shall examine how sensitive the results are to this choice.

In Fig. 4 we show the differential cross section per unit mass number as a function of p_T for various values of $P_{\rm lab}$ but without six-quark clusters ($f_{\rm Au} = 0.00$). The curves are similar to those obtained for a collision between two protons but with the nonisoscalarity correction included. The cross section decreases rapidly with p_T. If p_T is fixed, the cross section is higher for greater values of the laboratory momentum. The inclusion of six-quark clusters with $f_{\rm Au} = 0.30$, shown in Fig. 5, forces the cross

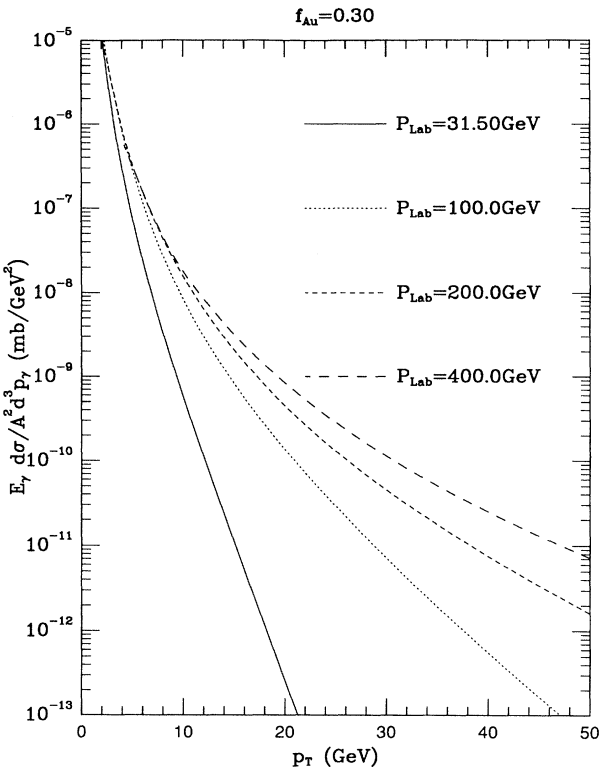

FIG. 5. Direct-photon production cross section for Au-Au collisions with six-quark clusters ($f_{\rm Au} = 0.30$) as a function of p_T.

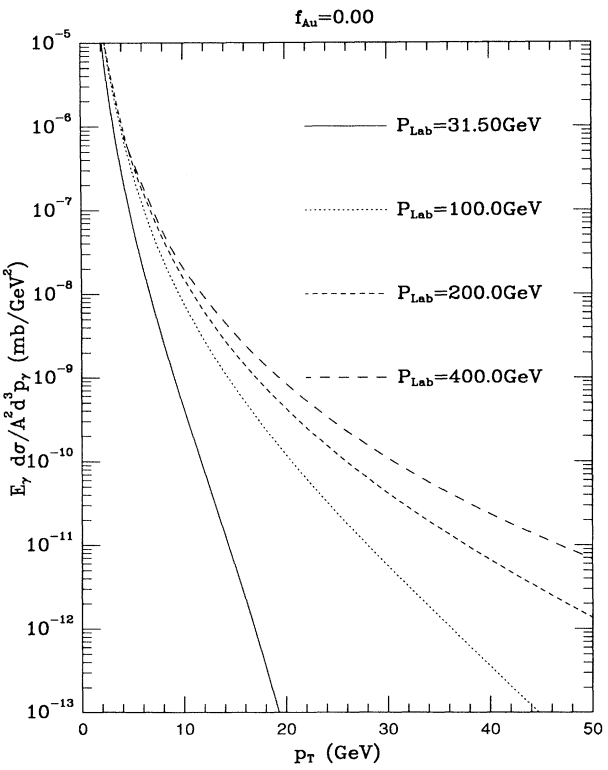

FIG. 4. Direct-photon production cross section for Au-Au collisions without six-quark clusters as a function of p_T.

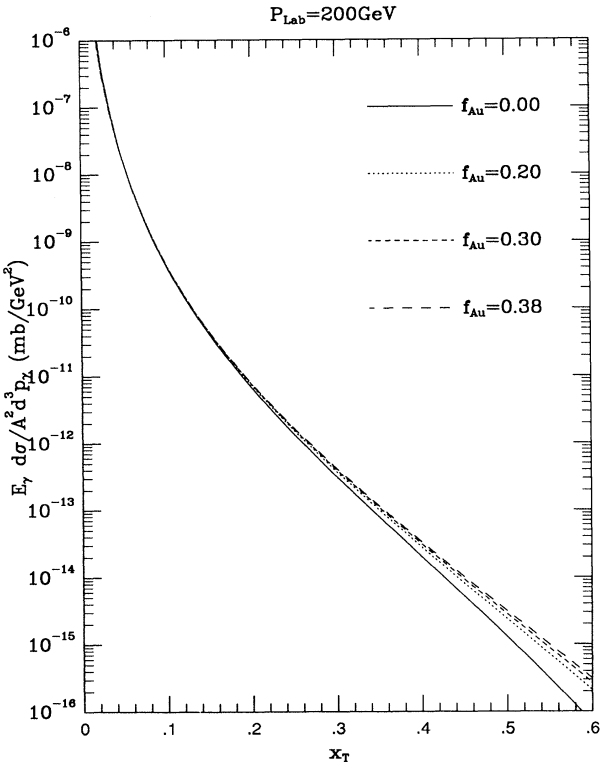

FIG. 6. Direct-photon production cross section for Au-Au collisions versus x_T for various values of $f_{\rm Au}$.

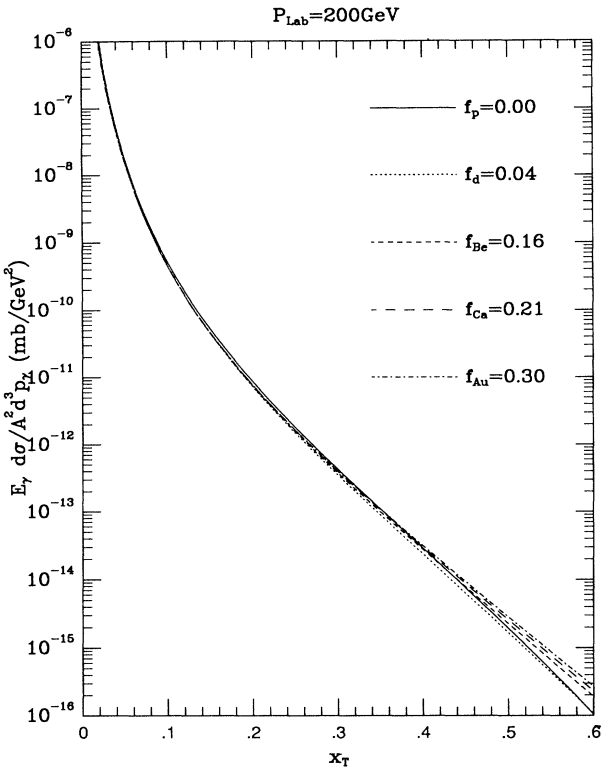

FIG. 7. Direct-photon production cross section for various nuclei versus x_T. The proton (p) case is shown for reference. Isoscalar (d, Ca) and nonisoscalar nuclei (Be, Au) are presented.

section to drop more slowly.

In Fig. 6 we plot the cross section versus x_T for $P_{\rm lab} = 200$ GeV and for various values of the six-quark cluster probability $f_{\rm Au}$. Clearly, as $f_{\rm Au}$ increases, the cross section increases. This conclusion holds for all values of $P_{\rm lab}$.

The cross section also increases with the mass number A as shown in Fig. 7 in which we plot it for various colliding nuclei. This dependence enters through the probability f. The nonisoscalarity correction is also present. The values of the six-quark cluster probabilities, in this figure, are chosen to follow the rule $f_A = 0.0575 \ln A$ with $f_d = 0.04$ (deuteron) taken as a starting point. Similar curves are obtained for all values of $P_{\rm lab}$.

When viewed on a semilog scale over many decades, the dependence of absolute cross sections on the presence of $6q$ clusters may appear to be rather weak. The same comment applies to the original EMC effect. Hence, the best way to observe these differences is through ratios of cross sections.

VII. CROSS SECTION RATIOS FOR $y = 0$

The influence of multiquark clusters is more clearly shown in ratios of differential cross sections per unit mass number for large nuclei relative to those for proton-proton collisions. Additionally, in ratios, the QCD evolution Q^2 dependence will tend to cancel as will, therefore, dependence on the factorization scale. Thus, we calculate the photon production ratio

$$R_\gamma = \frac{1}{A^2} \frac{d\sigma(A-A)/d^3p_\gamma}{d\sigma(p-p)/d^3p_\gamma}, \tag{39}$$

for gold relative to protons for various values of the six-quark cluster probability $f_{\rm Au}$.

Our calculations for $P_{\rm lab} = 100$, 200, and 400 GeV show that the curves for R_γ vs p_T shift towards larger p_T as $P_{\rm lab}$ increases. However, for a given $f_{\rm Au}$ value, as shown in Fig. 8, the different $P_{\rm lab}$ curves collapse to the same R_γ vs x_T curve, exhibiting x_T scaling as x_T is the relevant argument in parton structure functions for direct-photon production.

We observe that there is a striking x_T dependence of R_γ, reminiscent of the EMC effect in lepton DIS with $R_\gamma < 1.0$ at $x_T \leq 0.3$ to 0.4. The precise x_T value at which the ratio crosses unity decreases as $f_{\rm Au}$ increases. There is a local maximum at $x_T \approx 0.07$–0.08. For smaller x_T, the ratio decreases rapidly and increases monotonically for $x_T \geq 0.3$–0.4, becoming significantly greater than unity. This effect becomes more pronounced as $f_{\rm Au}$ increases, which increasingly contrasts with the curve for $f_{\rm Au} = 0.00$. The latter decreases monotonically and lies below unity as x_T increases.

Similar ratios to Eq. (39) can be calculated for a light nucleus in the denominator, e.g., the gold to deuteron cross section ratio shown in Fig. 9. Its behavior is similar to that of the gold to proton cross section ratio. How-

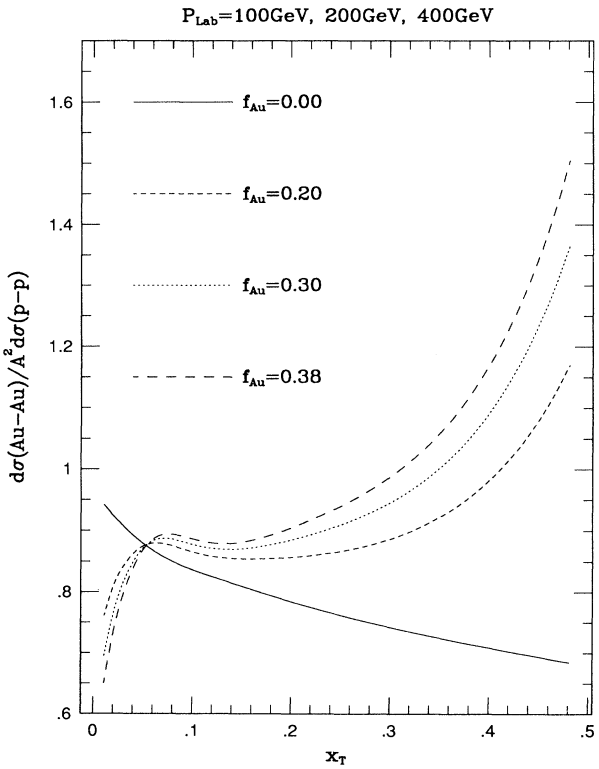

FIG. 8. Cross section ratio for direct-photon production as a function of x_T for various values of $f_{\rm Au}$. The curves scale in x_T.

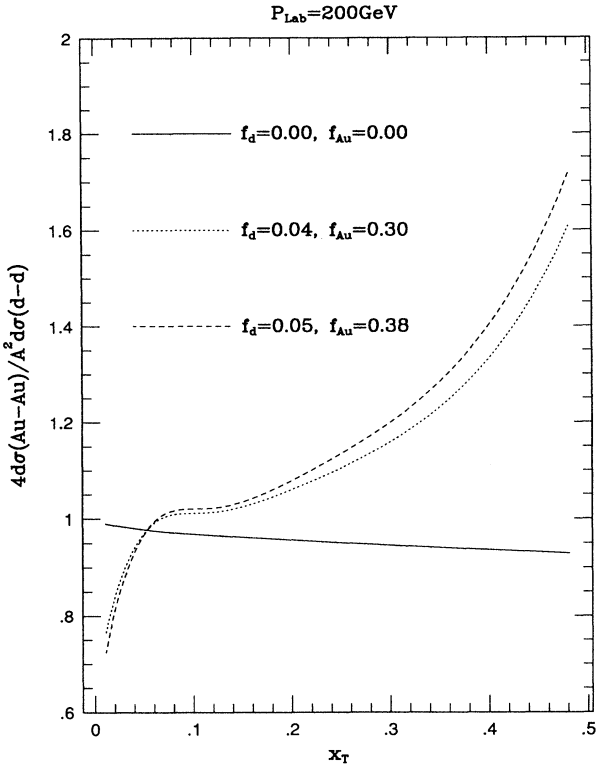

FIG. 9. Cross section ratio for direct-photon production as a function of x_T for various values of $f_{\rm Au}$ and f_d.

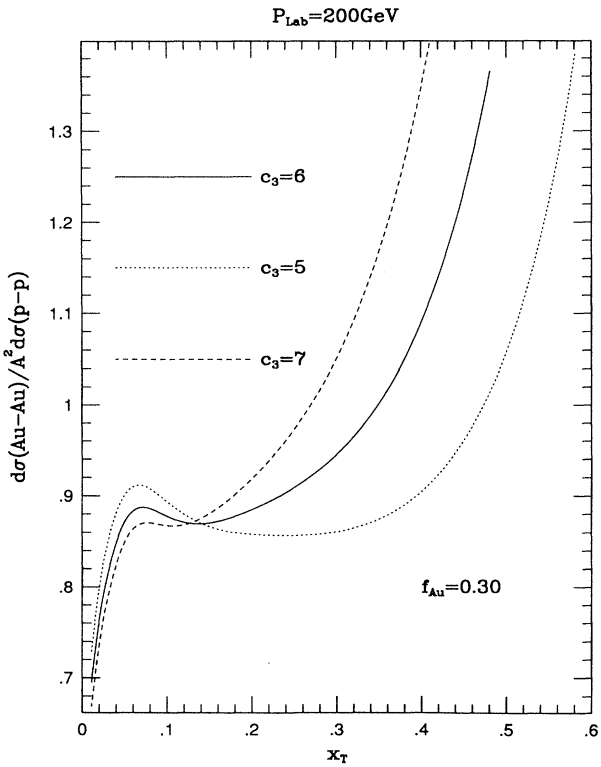

FIG. 10. Cross section ratio for direct-photon production as a function of x_T for various values of the three-quark cluster gluon exponent c_3 for $c_6 = 10$.

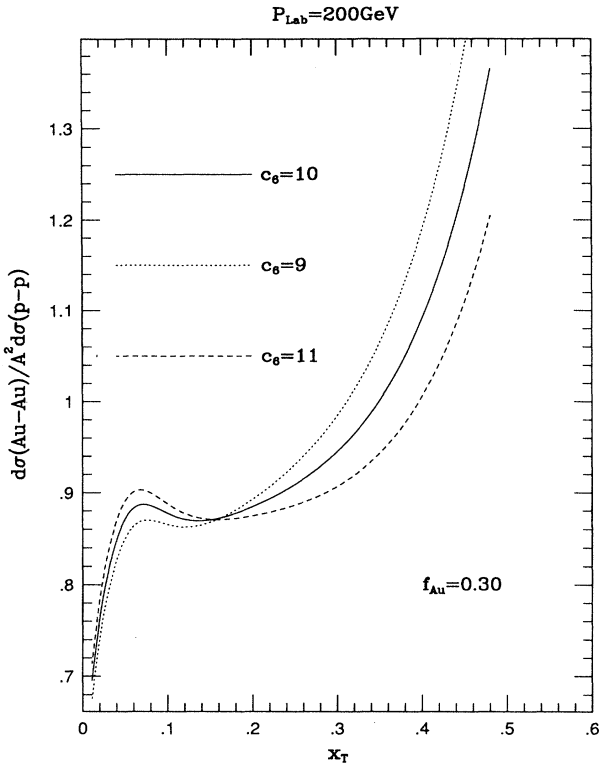

FIG. 11. Cross section ratio for direct-photon production as a function of x_T for various values of the six-quark cluster gluon exponent c_6 for $c_3 = 6$.

ever, it crosses over to values greater than 1 at $x_T \approx 0.1$. The curve for $f_d = f_{\rm Au} = 0.00$ is also presented for reference. The values of the six-quark cluster probabilities are consistent with a logarithmic dependence on the mass number. If the numerator referred to an isoscalar nucleus (A) and the denominator referred to a deuteron with $f_d = f_A = 0.00$, the curve would be a straight line, $R_\gamma = 1$.

The gluon distribution functions are the least known and yet an important component of our model. The shape of these distributions is determined by the exponents c_3 and c_6 of $(1-x)$. It is necessary to investigate the behavior of the R_γ when these parameters are changed from the initial choices $c_3 = 6$ and $c_6 = 10$. In Fig. 10 we show R_γ for $f_{\rm Au} = 0.30$, $c_6 = 10$ and $c_3 = 5$, 6, and 7. We observe that for $x_T \leq 0.14$ the ratio increases as c_3 decreases. The opposite happens for $x_T > 0.14$. This effect is quite marked for large x_T.

In Fig. 11 we present R_γ with $c_3 = 6$ fixed and letting $c_6 = 9$, 10, and 11, for $f_{\rm Au} = 0.30$. For $x_T \leq 0.18$ increasing c_6 results in higher R_γ. The effect is reversed for $x_T > 0.18$. The curves in Figs. 10 and 11 are plotted for $P_{\rm lab} = 200$ GeV, but exhibit x_T scaling, as implied by Fig. 8.

VIII. DISCUSSION

In this section we discuss the physical interpretation of our results. For all x_T, the quark-antiquark contribution

to the cross section is one to two orders of magnitude smaller than that of the quark-gluon term. Consequently, we first examine the x_T dependence of the cross section ratio R_γ shown in Fig. 8 at the limits $x_T \to 0$ and $x_T \to 1$. Particularly, we are interested in the f^2 part of the cross sections in R_γ.

For interactions of two three-quark clusters, we find ($x_2 \equiv x^{(j=3)}$), from Eqs. (36) and (37),

$$x^{(i=3)} = \frac{x_2 x_T}{2x_2 - x_T} \equiv x_1, \tag{40}$$

$$x_{\min}^{(j=3)} = \frac{x_T}{2 - x_T} \equiv x_{2(\min)}. \tag{41}$$

Then, as $x_T \to 1$,

$$x_1 \to \frac{x_2}{2x_2 - 1}, \quad x_{2(\min)} \to 1. \tag{42}$$

In this limit the integration over x_2 covers only an infinitesimal range. On the other hand, as $x_T \to 0$,

$$x_1 \to 0, \quad x_{2(\min)} \to 0. \tag{43}$$

In this limit the integration over x_2 covers the entire range from 0 to 1.

For interactions of two six-quark clusters, we find ($x^{(j=6)} \equiv z_2$)

$$x^{(i=6)} = \frac{z_2 x_T}{4z_2 - x_T} \equiv z_1, \tag{44}$$

$$x_{\min}^{(j=6)} = \frac{x_T}{4 - x_T} \equiv z_{2(\min)}. \tag{45}$$

Then, as $x_T \to 1$,

$$z_1 \to \frac{z_2}{4z_2 - 1}, \quad z_{2(\min)} \to \frac{1}{3}. \tag{46}$$

In this limit the integration over z_2 covers a reduced but nonzero range. On the other hand, as $x_T \to 0$,

$$z_1 \to 0, \quad z_{2(\min)} \to 0. \tag{47}$$

In this limit the integration over z_2 covers the entire range from 0 to 1.

Since when x_T is small x_1 (or z_1) is also small and when x_T is large x_1 (or z_1) is also large, the hard cross section for quark-gluon scattering does not vary much with x_T. Consequently, the convoluted quark-gluon hadronic structure functions determine the essential behavior of R_γ. Then, in the limit $x_T \to 1$, the f^2 term in R_γ,

$$\left(\frac{f}{1+f}\right)^2 \frac{\int_{1/3}^1 dz_2 g_6(z_1) g_6(z_2)/(z_2 s + t)}{\int_{\approx 1}^1 dx_2 g_3(x_1) g_3(x_2)/(x_2 s + t)}$$

tends to infinity. This is a phase space effect whereby the more massive six-quark clusters can produce photons more copiously at high p_T. Without the presence of the f^2 term, the cross section ratio would flatten out as $x_T \to 1$, tending to a value greater than 1, as shown by Petridis [12].

In the limit $x_T \to 0$ the gluon distributions for the positively moving nucleus are calculated at $x_1 = z_1 = 0$ where they are equal to the product of the total momentum fractions carried by the gluons in the corresponding clusters and the factor $(c_{3,6} + 1)$. The integration over x_2 or z_2 in the range from 0 to 1 depends on the exponents c_3 and c_6 which determine the shape of the gluon distributions. From the values for these exponents in Table I,

$$R_\gamma(0) \approx \frac{1 + 1.204f + 0.362f^2}{1 + 2f + f^2}, \tag{48}$$

a decreasing function of f. It should be noted that this expression neglects the $q\bar{q}$ contribution. Clearly, for $f = 0$, $R_\gamma(0) = 1$, as expected.

We conclude that the small x_T behavior of the cross section ratio depends largely on the shape of the gluon distributions and the total momentum fraction carried by gluons.

The presence of the $q\bar{q}$ annihilation terms can be seen in nonisoscalar nuclei for $f = 0$ as shown in the solid curves in Figs. 8 and 9. These contain more neutron-type clusters which implies more *down* valence quarks whose momentum distributions are concentrated towards smaller values of the quark momentum fraction x than those of *up* quarks. This lowers $R_\gamma(1)$.

As we have pointed out, $R_\gamma(0)$ is sensitive to the relative values of c_3 and c_6. Higher values of these exponents describe *softer* gluon distributions. The effects of changing c_3 and c_6 should be opposite due to the fact that the six-quark clusters appear mostly in the numerator of the cross section ratios (compare the curves in Fig. 10 as c_3 increases with those given in Fig. 11 for increasing c_6). Momentum conservation balances the behavior of R_γ between small and large x_T as the exponents are altered.

The cross section ratio scales in x_T implying that the expectation value of the transverse momentum is proportional to $P_{\rm lab}$. This reflects the pointlike nature of the interacting partons in a way similar to the Bjorken scaling in lepton deep inelastic scattering on nucleons. In fact we may define the expectation value of p_T for zero photon longitudinal rapidity as

$$\langle p_T \rangle_{y=0} = \frac{\sum_{i,j=3,6} \int_{p_{T\min}}^{p_{T\max}(i,j)} dp_T \, p_T \, E_\gamma d\sigma^{(i,j)}(y=0)/d^3 p_\gamma}{\sum_{i,j=3,6} \int_{p_{T\min}}^{p_{T\max}(i,j)} dp_T \, E_\gamma d\sigma^{(i,j)}(y=0)/d^3 p_\gamma}, \tag{49}$$

where $E_\gamma d\sigma^{(i,j)}(y=0)/d^3 p_\gamma$ are the hadronic level cross sections for interaction between i,j-type clusters after integration over $x^{(i)}$ and $x^{(j)}$. The upper integration limits depend on the cluster kinematics so that separate integrations must be performed for the four cluster interaction cases. The lower limit is chosen so that α_s remains positive. Numerical calculation of $\langle p_T \rangle$ shows that it is indeed proportional to $P_{\rm lab}$. The slope of $\langle p_T \rangle$ vs $P_{\rm lab}$ is

approximately 0.056 when six-quark clusters are present and a little lower when they are not. Upon integration over p_T the total cross section that appears in the denominator of Eq. (49) does not show any special features as a function of $P_{\rm lab}$.

The cross section for direct-photon production is affected by higher order QCD corrections. These include soft gluon emission [27] and bremsstrahlung of photons [26] off quarks. These processes have been studied thoroughly by other authors in the case of nucleon-nucleon collisions [28]. Their results indicate that they do not affect *ratios* of cross sections significantly.

As a final summary, we note that the cross section ratios for direct-photon production in gold-gold collisions compared with proton-proton (deuteron-deuteron) collisions plotted in Fig. 8 (9) are dramatically different when allowing for the presence of multiquark clusters in nuclei. This source of photon emission in relativistic heavy-ion collisions is implied by the existence of the EMC effect and will have to be taken into account before claiming evidence of photons from the quark-gluon plasma.

ACKNOWLEDGMENTS

The authors are especially grateful to Jianwei Qiu for numerous helpful conversations. One of the authors (K.E.L.) would like to thank Patrick Aurenche for useful comments; he also acknowledges support through the U.S. and Polish National Academy of Sciences exchange program and the hospitality of the Institute of Theoretical Physics, Warsaw University, and the Soltan Institute in Warsaw. This work was supported by the U.S. Department of Energy under Contracts No. DE-FG02-87ER40371 and No. W-7405-ENG-82 Office of Energy Research (KA-01-01), Division of High Energy and Nuclear Physics.

APPENDIX

The explicit forms of the eight hadronic structure functions that appear in the hadron level cross section are given as sums of products of the parton number densities weighted by the numbers of each type of quark cluster involved and the squares of the quark charges. The notation is introduced in the main body of this article. The variables x_1 and x_2 refer to the momentum fractions carried by the interacting partons from the first nucleus, moving in the positive z direction, and the second nucleus, moving in the negative z direction, respectively. The superscripts refer to the types of clusters involved. The subscripts refer to the hard process. Isospin invariance relations have been used in the derivation of these formulas.

The four hadronic structure functions for the quark-antiquark annihilation process are

$$\begin{aligned} H_{q\bar{q}}^{(3,3)}(x_1,x_2) = &\left[\left\{\frac{4}{9}n_p^2+\frac{5}{9}n_pn_n+\frac{1}{9}n_n^2\right\}u_3(x_1)+\left\{\frac{1}{9}n_p^2+\frac{5}{9}n_pn_n+\frac{4}{9}n_n^2\right\}d_3(x_1)\right]s_3(x_2)\\ &+s_3(x_1)\left[\left\{\frac{4}{9}n_p^2+\frac{5}{9}n_pn_n+\frac{1}{9}n_n^2\right\}u_3(x_2)+\left\{\frac{1}{9}n_p^2+\frac{5}{9}n_pn_n+\frac{4}{9}n_n^2\right\}d_3(x_2)\right]\\ &+\frac{7}{6}n_3^2s_3(x_1)s_3(x_2), \end{aligned} \tag{A1}$$

$$\begin{aligned} H_{q\bar{q}}^{(3,6)}(x_1,x_2) = &\, n_6\left[\left\{\frac{4}{9}n_p+\frac{1}{9}n_n\right\}u_3(x_1)+\left\{\frac{1}{9}n_p+\frac{4}{9}n_n\right\}d_3(x_1)+\frac{7}{6}n_3s_3(x_1)\right]s_6(x_2)\\ &+n_3s_3(x_1)\left[\left\{\frac{4}{9}n_{pp}+\frac{5}{18}n_{pn}+\frac{1}{9}n_{nn}\right\}u_6(x_2)+\left\{\frac{1}{9}n_{pp}+\frac{5}{18}n_{pn}+\frac{4}{9}n_{nn}\right\}d_6(x_2)\right], \end{aligned} \tag{A2}$$

$$\begin{aligned} H_{q\bar{q}}^{(6,3)}(x_1,x_2) = &\, n_3\left[\left\{\frac{4}{9}n_{pp}+\frac{5}{18}n_{pn}+\frac{1}{9}n_{nn}\right\}u_6(x_1)+\left\{\frac{1}{9}n_{pp}+\frac{5}{18}n_{pn}+\frac{4}{9}n_{nn}\right\}d_6(x_1)+\frac{7}{6}n_6s_6(x_1)\right]s_3(x_2)\\ &+n_6s_6(x_1)\left[\left\{\frac{4}{9}n_p+\frac{1}{9}n_n\right\}u_3(x_2)+\left\{\frac{1}{9}n_p+\frac{4}{9}n_n\right\}d_3(x_2)\right], \end{aligned} \tag{A3}$$

and, finally,

$$\begin{aligned} H_{q\bar{q}}^{(6,6)}(x_1,x_2) = &\, n_6\left[\left\{\frac{4}{9}n_{pp}+\frac{5}{18}n_{pn}+\frac{1}{9}n_{nn}\right\}u_6(x_1)+\left\{\frac{1}{9}n_{pp}+\frac{5}{18}n_{pn}+\frac{4}{9}n_{nn}\right\}d_6(x_1)\right]s_6(x_2)\\ &+n_6s_6(x_1)\left[\left\{\frac{4}{9}n_{pp}+\frac{5}{18}n_{pn}+\frac{1}{9}n_{nn}\right\}u_6(x_2)+\left\{\frac{1}{9}n_{pp}+\frac{5}{18}n_{pn}+\frac{4}{9}n_{nn}\right\}d_6(x_2)\right]\\ &+\frac{7}{6}n_6^2s_6(x_1)s_6(x_2). \end{aligned} \tag{A4}$$

The four hadronic structure functions for the quark-gluon Compton scattering process are

$$H_{qg}^{(3,3)}(x_1,x_2) = g_3(x_1)\left[\left\{\frac{4}{9}n_p^2+\frac{5}{9}n_pn_n+\frac{1}{9}n_n^2\right\}u_3(x_2)+\left\{\frac{1}{9}n_p^2+\frac{5}{9}n_pn_n+\frac{4}{9}n_n^2\right\}d_3(x_2)+\frac{11}{9}n_3^2s_3(x_2)\right]$$
$$+\left[\left\{\frac{4}{9}n_p^2+\frac{5}{9}n_pn_n+\frac{1}{9}n_n^2\right\}u_3(x_1)+\left\{\frac{1}{9}n_p^2+\frac{5}{9}n_pn_n+\frac{4}{9}n_n^2\right\}d_3(x_1)+\frac{11}{9}n_3^2s_3(x_1)\right]g_3(x_2), \quad \text{(A5)}$$

$$H_{qg}^{(3,6)}(x_1,x_2) = n_3g_3(x_1)\left[\left\{\frac{4}{9}n_{pp}+\frac{5}{18}n_{pn}+\frac{1}{9}n_{nn}\right\}u_6(x_2)+\left\{\frac{1}{9}n_{pp}+\frac{5}{18}n_{pn}+\frac{4}{9}n_{nn}\right\}d_6(x_2)+\frac{11}{9}n_6s_6(x_2)\right]$$
$$+n_6\left[\left\{\frac{4}{9}n_p+\frac{1}{9}n_n\right\}u_3(x_1)+\left\{\frac{1}{9}n_p+\frac{4}{9}n_n\right\}d_3(x_1)+\frac{11}{9}n_3s_3(x_1)\right]g_6(x_2), \quad \text{(A6)}$$

$$H_{qg}^{(6,3)}(x_1,x_2) = n_6g_6(x_1)\left[\left\{\frac{4}{9}n_p+\frac{1}{9}n_n\right\}u_3(x_2)+\left\{\frac{1}{9}n_p+\frac{4}{9}n_n\right\}d_3(x_2)+\frac{11}{9}n_3s_3(x_2)\right]$$
$$+n_3\left[\left\{\frac{4}{9}n_{pp}+\frac{5}{18}n_{pn}+\frac{1}{9}n_{nn}\right\}u_6(x_1)+\left\{\frac{1}{9}n_{pp}+\frac{5}{18}n_{pn}+\frac{4}{9}n_{nn}\right\}d_6(x_1)+\frac{11}{9}n_6s_6(x_1)\right]g_3(x_2), \quad \text{(A7)}$$

and, finally,

$$H_{qg}^{(6,6)}(x_1,x_2) = n_6g_6(x_1)\left[\left\{\frac{4}{9}n_{pp}+\frac{5}{18}n_{pn}+\frac{1}{9}n_{nn}\right\}u_6(x_2)+\left\{\frac{1}{9}n_{pp}+\frac{5}{18}n_{pn}+\frac{4}{9}n_{nn}\right\}d_6(x_2)+\frac{11}{9}n_6s_6(x_2)\right]$$
$$+n_6\left[\left\{\frac{4}{9}n_{pp}+\frac{5}{18}n_{pn}+\frac{1}{9}n_{nn}\right\}u_6(x_1)+\left\{\frac{1}{9}n_{pp}+\frac{5}{18}n_{pn}+\frac{4}{9}n_{nn}\right\}d_6(x_1)+\frac{11}{9}n_6s_6(x_1)\right]g_6(x_2). \quad \text{(A8)}$$

[1] EMC, J. J. Aubert *et al.*, Phys. Lett. **123B**, 275 (1983); A. Bodek *et al.*, Phys. Rev. Lett. **50**, 1431 (1983); **51**, 534 (1983); R. G. Arnold *et al., ibid.* **52**, 727 (1984); G. Bari *et al.*, Phys. Lett. **163B**, 282 (1985); A. C. Benvenuti *et al.*, Phys. Lett. B **189**, 483 (1987); J. J. Aubert *et al.*, Nucl. Phys. **B259**, 189 (1985); **B272**, 158 (1986).

[2] See, e.g., the summary discussion and references in K. E. Lassila, in *Proceedings of the Fifth International Conference on Hadronic Mechanics and Non-potential Interactions,* Cedar Falls, Iowa, 1990, edited by R. B. Campbell and H. C. Myung (Nova, New York, 1991); see also [3] and [4].

[3] K. E. Lassila, A. N. Petridis, C. E. Carlson, and U. P. Sukhatme, in *The Rice Meeting,* Proceedings of the Annual Meeting of the Division of Particles and Fields of the APS, Houston, Texas, 1990, edited by B. Bonner and H. Miettinen (World Scientific, Teaneck, NJ, 1990), p. 593.

[4] K. E. Lassila, U. P. Sukhatme, A. Harindranath, and J. P. Vary, Phys. Rev. C **44**, 1188 (1991).

[5] H. J. Pirner and J. P. Vary, Phys. Rev. Lett. **46**, 1376 (1981); J. P. Vary, Nucl. Phys. **A418**, 195 (1984).

[6] C. E. Carlson and T. J. Havens, Phys. Rev. Lett. **51**, 261 (1983).

[7] K. E. Lassila and U. P. Sukhatme, Phys. Lett. B **209**, 343 (1988).

[8] J. P. Vary, S. A. Coon, and H. J. Pirner, in *Hadronic Probes and Nuclear Interactions (Physical Science Center at Arizona State University, Tempe, Arizona)*, Proceedings of the International Conference on Hadronic Probes and Nuclear Interactions, edited by J. R. Comfort, W. R. Gibbs, and B. G. Ritchie, AIP Conf. Proc. No. 133 (AIP, New York, 1985); L. S. Kisslinger, W. H. Ma, and P. Hoodbhoy, Nucl. Phys. **A459**, 645 (1986).

[9] K. E. Lassila and U. P. Sukhatme, in *Nuclear and Particle Physics on the Light Cone*, Proceedings of the Symposium, Los Alamos, New Mexico, 1988, edited by M. Johnson and L. Kisslinger (World Scientific, Singapore, 1989), p. 115.

[10] A. Harindranath and J. P. Vary, Phys. Rev. D **34**, 3378 (1986); see also [11].

[11] E. L. Berger, Nucl. Phys. **B267**, 231 (1986); R. P. Bickerstaff, M. C. Birse, and G. A. Miller, Phys. Rev. Lett. **53**, 2532 (1984); Phys. Rev. D **33**, 3228 (1986); W. P. Hwang and L. S. Kisslinger, Phys. Rev. D **38**, 788 (1988).

[12] K. E. Lassila, A. N. Petridis, U. P. Sukhatme, and G. Wilk, Phys. Lett. B **297**, 191 (1992); A. N. Petridis, Ph.D. thesis, Iowa State University, 1992.

[13] G. Yen and J. P. Vary, Phys. Rev. C **40**, R16 (1989); G. Yen, J. P. Vary, A. Harindranath, and H. J. Pirner, *ibid.* **42**, 1665 (1990).

[14] U. P. Sukhatme, G. Wilk, and K. E. Lassila, Z. Phys. C **53**, 439 (1992).

[15] C. E. Carlson, K. E. Lassila, and U. P. Sukhatme, Phys. Lett. B **263**, 277 (1991).

[16] M. Sato, S. A. Coon, H. J. Pirner, and J. P. Vary, Phys. Rev. C **33**, 1062 (1986).

[17] P. D. Morley and S. A. Williams, Z. Phys. A **331**, 239 (1988); P. D. Morley, D. L. Pursey, and S. A. Williams, Phys. Rev. C **42**, 2698 (1990); T. Goldman *et al.*, in *Nuclear Chromodynamics*, Proceedings of the Topical Conference, Argonne, Illinois, 1988, edited by J. Qiu and D. Sivers (World Scientific, Singapore, 1988), p. 1.

[18] F. Stancu and L. Wilets, Phys. Rev. C **36**, 726 (1987); **38**, 1145 (1988).

[19] A. Mueller and J. Qiu, Nucl. Phys. **B268**, 427 (1986); J. Qiu, *ibid.* **B291**, 746 (1987).

[20] T. Ferbel and W. Molzon, Rev. Mod. Phys. **56**, 181 (1984).

[21] T. Ferbel, in *Puzzles on the Electroweak Scale*, Proceedings of the 14th International Warsaw Symposium on Elementary Particle Physics, Warsaw, Poland, 1991, edited by Z. Ajduk, S. Pokorski, and A. K. Wroblewski (World Scientific, Singapore, 1992), p. 563.
[22] E. Shuryak, Yad. Fiz. **28**, 796 (1978) [Sov. J. Nucl. Phys. **28**, 408 (1978)]; E. L. Feinberg, Nuovo Cimento A **34**, 391 (1976).
[23] M. Virchaux (unpublished); W. K. Tung (unpublished).
[24] U. P. Sukhatme (private communication).
[25] F. Halzen and D. Scott, Phys. Rev. D **18**, 3378 (1978); F. Halzen and D. Scott, Phys. Rev. Lett. **40**, 1117 (1978).
[26] E. Berger and J. Qiu, Phys. Rev. D **44**, 2002 (1991), and references therein.
[27] A. Contogouris, S. Papadopoulos, and J. Ralston, Phys. Lett. **140B**, 70 (1981).
[28] P. Aurenche, R. Baier, M. Fontannaz, and D. Schiff, Nucl. Phys. **B297**, 661 (1988); P. Aurenche, R. Baier, M. Fontannaz, J. Owens, and M. Werlen, Phys. Rev. D **39**, 3275 (1989), and references therein.